

The Impact of Precursor Ratio on the Synthetic Production, Surface Chemistry, and Photovoltaic Performance of CsPbI₃ Perovskite Quantum Dots

Yuli Qian, Yao Shi, Guangyi Shi, Guozheng Shi,* Xuliang Zhang, Lin Yuan, Qixuan Zhong, Yang Liu, Yao Wang, Xufeng Ling, Fangchao Li, Muhan Cao, Shaojuan Li, Qiao Zhang, Zeke Liu,* and Wanli Ma*

Lead-halide perovskite quantum dots (QDs) have attracted substantial attention due to their great potential in solution-processed optoelectronic applications. The current synthetic method mostly relies on the binary-precursor strategy, which significantly restricts the reaction yield and elemental regulation, leading to extremely high material cost. Herein, a more versatile ternary-precursor method to investigate the effect of the precursor ratios on the synthetic production, surface chemistry, and photovoltaic performance of CsPbI₃ QDs is explored. It is revealed that a decreased Pb/Cs feeding ratio can largely increase the reaction yield, whereas a reduced Pb/I ratio can improve the surface termination and optical properties of the resultant CsPbI₃ QDs. After rational tuning of the synthetic protocol, the reaction yield can be improved more than 7.5 times and the material cost can be reduced from 303 \$ g⁻¹ to as low as 42 \$ g⁻¹ compared to the conventional binary-precursor method. In addition, the photovoltaic device using these QDs exhibits an efficiency close to the reported state-of-the-art ones. It is believed that this scalable and low-cost preparation of CsPbI₃ QDs provides new insight into the future commercialization of perovskite QDs-based optoelectronics.

1. Introduction

All-inorganic CsPbX₃ (X = Cl, Br, I) perovskite quantum dots (QDs) are emerging types of semiconductor nanomaterials in addition to the traditional IV–VI and III–V QDs (CdSe, PbS, InP, etc.).^[1–5] CsPbX₃ QDs exhibit excellent optical properties such as high photoluminescence quantum yields (PLQYs), narrow full width at half-maximum (FWHM), and tunable bandgaps, which is comparable or even superior to state-of-the-art CdSe QDs with sophisticated shelling or surface passivation, showing huge potential for lighting/display applications.^[1,2,5–11] Recently, it was demonstrated that CsPbI₃ QDs can keep a stable black phase at room temperature,^[12] whereas bulk CsPbI₃ will convert to a nonperovskite yellow phase (δ -phase) with unfavorable optoelectronic properties at the temperature below 320 °C. In addition to the extraordinary phase stability,

CsPbI₃ QDs also possess superior thermal stability over the widely studied organic–inorganic hybrid perovskites.^[13,14] Furthermore, among all Pb-based inorganic perovskites QDs, CsPbI₃ QDs possess the lowest bandgap (≈ 1.8 eV) to sufficient utilization of solar energy, which make them desired building blocks for photovoltaic application. After the pioneering report of CsPbI₃ QDs solar cells with a power conversion efficiency (PCE) of 10.77% by Luther and his co-workers in 2016,^[12] the device performance was rapidly improved to 16.1% for CsPbI₃ QD^[15] and 16.6% for Cs_{1-x}FA_xPbI₃ (FA: formamidinium)^[16] QD solar cells. Moreover, perovskite QDs solar cells can offer additional advantages in scalable manufacturing, such as using industrially friendly solvents, improved film quality, and flexible heterojunction or tandem device structures.^[17,18] Resultantly, CsPbI₃ QDs solar cells have attracted substantial interest in the field of photovoltaics during the past few years.^[12,16,17,19–30]

Nowadays, almost all CsPbX₃ QDs applied in solar cells are synthesized by the hot injection method developed by Protesescu et al. in 2015,^[31] in which, PbX₂ is dissolved in octadecene containing oleylamine (OLA) and oleic acid (OA) as ligands. After injecting the Cs precursor, high-quality CsPbX₃

Y. Qian, Y. Shi, G. Shi, Dr. G. Shi, X. Zhang, L. Yuan, Q. Zhong, Y. Liu, Y. Wang, X. Ling, Dr. F. Li, Prof. M. Cao, Prof. Q. Zhang, Prof. Z. Liu, Prof. W. Ma

Institute of Functional Nano & Soft Materials (FUNSOM)

Jiangsu Key Laboratory for Carbon-Based Functional Materials and Devices

Joint International Research Laboratory of Carbon-Based Functional Materials and Devices

Soochow University

199 Ren-Ai Road, Suzhou Industrial Park, Suzhou, Jiangsu 215123, P. R. China

E-mail: gzshi@suda.edu.cn; zkliu@suda.edu.cn; wlma@suda.edu.cn

Prof. S. Li, Prof. Z. Liu

State Key Laboratory of Applied Optics

Changchun Institute of Optics

Fine Mechanics and Physics

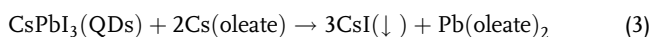
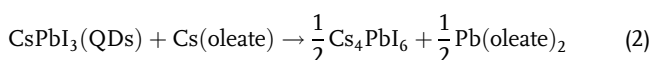
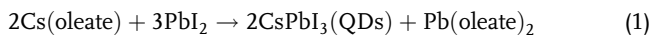
Chinese Academy of Sciences

Changchun 130033, China

 The ORCID identification number(s) for the author(s) of this article can be found under <https://doi.org/10.1002/solr.202100090>.

DOI: 10.1002/solr.202100090

QDs with relatively homogeneous sizes can be formed (Figure 1a, Figure S1, Supporting Information, reaction (1)). However, using PbX_2 as both lead cation and halide anion precursors leads to two serious disadvantages: 1) high Pb/Cs ratio (usually in the range of 3.2–7.5) is a prerequisite to acquiring high-quality CsPbX_3 QDs,^[32] leading to undesired Pb waste and low synthetic yield, which can be attributed to the by-reactions triggered by Cs-oleate in reaction (2) and (3).^[22]



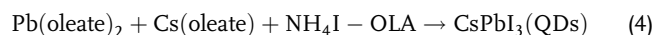
Therefore, excess PbI_2 has to be used to fully convert Cs-oleate and avoid the by-reactions. The low synthetic production can severely impede high-throughput research and mass manufacturing. 2) The feeding ratio of lead to halide cannot be tuned due to the fixed stoichiometry of PbX_2 . Nevertheless, the element ratios in precursors can make a significant impact on the properties of CsPbX_3 QDs,^[33,34] and also proven to be critical in bulk perovskite thin-film solar cells.^[35–37] Thus, alternative synthetic protocol with more tunability in precursor feed ratios should be adopted.

Consequently, several ternary-precursor methods have been developed.^[38–40] In these protocols, the precursors for each element (Cs, Pb, and halide) are independent, which endows the capability to study the effect of precursor feeding ratios on the optoelectronic properties of CsPbX_3 QDs. The halide-rich synthetic condition has proven to be beneficial for light-emitting diode (LED) based on CsPbX_3 QDs.^[38–41] In addition, the halide-rich condition can also ensure the phase purity of synthesized CsPbX_3 QDs under a low Pb/Cs ratio, which may be an effective pathway to increase synthetic yield and reduce lead waste. However, so far there are still no such investigations conducted on CsPbI_3 QDs solar cells.

In this article, we systematically tuned the feeding ratios in the synthesis of CsPbI_3 QDs using ternary-precursor method, and revealed the effect of both Pb/Cs and Pb/I ratios on the synthetic yield and optoelectronic properties of the obtained QDs. It was found that the demand for excess Pb precursor in the conventional binary-precursor method can be largely relieved in the ternary-precursor protocol. A low ratio of Pb/Cs = 1 was adequate to maximize the utilization of cation precursors. Resultantly, the synthetic yield was improved more than 7.5 times, and the synthesis cost was simultaneously reduced to 14% of the conventional binary-precursor method under the same Pb feeding. Meanwhile, we found that the different feeding Pb/I ratios can affect the surface bonding motifs of the obtained QDs and then influenced their optoelectronic properties. After accordingly modified surface treatment, the PCE of the control devices is close to those based on CsPbI_3 QDs synthesized using the binary-precursor method. We believe the significantly increased synthetic production and reduced preparation cost of CsPbI_3 QDs will be beneficial for the large-scale fabrication of efficient optoelectronic devices based on perovskite QDs.

2. Results and Discussion

The ternary-precursor strategy was conducted by modifying the reported recipe.^[34] $\text{PbAc}_2 \cdot 3\text{H}_2\text{O}$ and Cs_2CO_3 were dissolved in 1-octadecene (ODE) containing OA and OLA as the precursors for Pb and Cs, respectively. Then, the degassed mixture of NH_4I and OLA was injected into the solution at 180 °C to trigger the reaction (reaction (4), Figure 1b). The ratios of all three precursors can be independently tuned.



Theoretically, the feeding ratio of Cs:Pb:I = 1:1:3 can maximize the utilization of the precursors. However, it was observed that by-product Cs_4PbI_6 can be formed under this feeding ratio (Figure S2, Supporting Information). Increasing the Cs:Pb:I ratio to 1:1:5 can produce almost phase-pure CsPbI_3 QDs, but

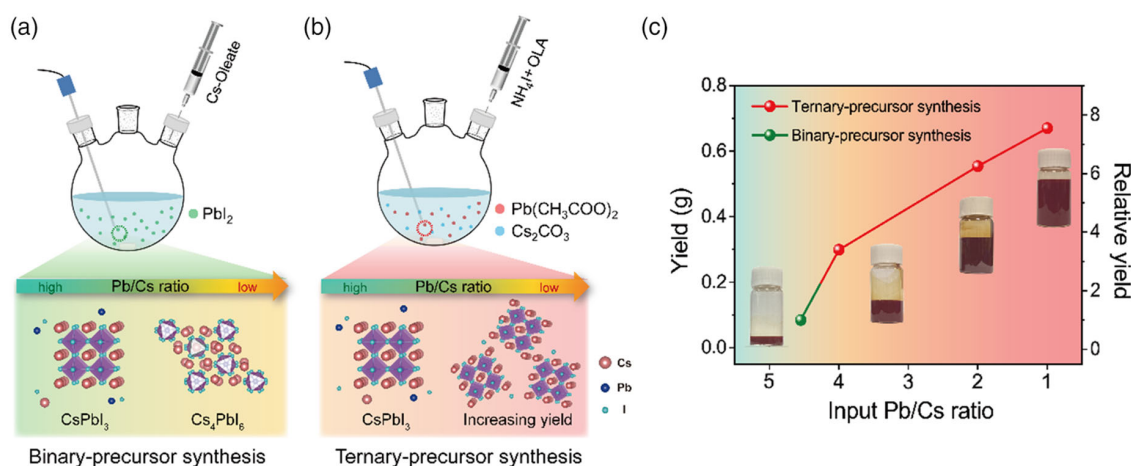


Figure 1. Illustration of synthesis based on a) binary-precursor method and b) ternary-precursor method. c) Yield of the CsPbI_3 QDs synthesized with different methods and input ratios. Inset: photographs of the obtained CsPbI_3 QDs in octane with a concentration of 70 mg mL^{-1} . The input Pb precursors are all fixed at 2.16 mmol.

with aggregations. The CsPbI₃ QDs with both high phase purity and decent dispersibility can be achieved at a ratio of Cs:Pb: I = 1:1:6 (Figure S2, Supporting Information). We further systematically investigated the effect of precursor feeding ratios on the crystalline phases of the obtained QDs. As shown in Table S1, Supporting Information, the high demand for iodide precursors to obtain pure-phase CsPbI₃ QDs can be lowered under an increased Pb/Cs ratio. These results are in accordance with the previous studies that excessive Cs precursor (Cs-oleate) in the system tends to trigger the by-reaction (reaction 2).^[32] Therefore, excessive PbI₂ is necessary to fully consume Cs-oleate in the conventional binary-precursor synthesis. However, this requirement can be relieved if the supplied iodide is sufficient.^[22] According to Le Chatelier's principle, increasing the supply of either reactant can drive the reaction to the product's side. Thus, either Pb or iodide has to be supplied excessively, whereas the feed of excessive iodide instead of Pb is more advisable considering the toxicity of Pb.

Since PbI₂ has to be largely excessive (Pb/Cs = 4.55 in most reactions) in the conventional binary-precursor synthesis,^[31] and only 2/3 of Pb can be utilized according to the reaction (1). Then, only ≈15% of the total Pb can be converted into CsPbI₃, which largely restricts the reaction yield. In the ternary-precursor strategy, the sufficient iodide supply can ensure higher utilization of cations. Therefore, the reaction yield of the ternary-precursor synthesis can be substantially improved. The reaction with a Pb/Cs ratio of 1 can convert all cations into the final products and show the highest reaction yield. Theoretically, the yield of the reaction with Pb/Cs = 1 should be ≈6.7 times higher than that of the conventional binary-precursor reaction, assuming all Cs can be converted. To prove that, we conducted a series of ternary-precursor syntheses with varying Pb/Cs ratios while keeping a constant amount of Pb. After synthesis, we took the same amount of crude solution from each reaction and equally diluted them (Figure S3a, Supporting Information). The relative absorption intensity at 670 nm (close to the absorption edge, representing the amount of CsPbI₃ QDs) enhances with increased Cs feeding and is almost proportional to the Cs/Pb ratio in the ternary-precursor synthesis (Figure S3b, Supporting Information).

For the fabrication of solar cells, the QDs have to be purified at least twice to fully remove the excess solvent and ligands (Figure S4, Supporting Information).^[42] Unlike the purification of traditional II–VI and IV–VI QDs, the antisolvent (methyl acetate, MeOAc) used in the purification of CsPbI₃ QDs is relatively nonpolar and the amount of antisolvent has to be finely adjusted due to the fragile feature of CsPbI₃ QDs. The attempt to increase yield by using higher polarity or a larger amount of antisolvent will lead to damaged CsPbI₃ QDs.^[43] As a result, a fair amount of the product cannot be precipitated and collected. Meanwhile, the purification process can inevitably cause some QDs to agglomerate due to the excessive removal of ligands. The aggregated QDs will be centrifuged and removed before device fabrication, leading to further reduced production yield. The reaction with 1 g PbI₂ (2.16 mmol) reactant can only produce ≈80 mg high quality CsPbI₃ QDs for solar cell fabrication in the conventional binary-precursor synthesis. This low yield renders the cost of CsPbI₃ QDs up to ≈303 \$ g⁻¹ (Table S2, Supporting Information). As we have demonstrated, the yield of CsPbI₃ QDs synthesized

using the ternary-precursor method can be substantially improved with decreased Pb/Cs ratio (Figure 1c). Resultantly, 610 mg CsPbI₃ QDs can be obtained for the ternary-precursor reaction with Pb/Cs = 1 under the same molar Pb feeding, which is more than 7.5 times higher than that of the conventional two-precursor synthesis. The cost for the preparation of CsPbI₃ QDs is then reduced to as low as 42 \$ g⁻¹ (Table S3 and S4, Supporting Information), which is significantly cheaper compared to that of the conventional two-precursor synthesis (≈303 \$ g⁻¹) (Table S2, Supporting Information). And, the reaction can be scaled up at least four times with an almost linear increase in reaction yield (Figure S5, Supporting Information). As a conclusion, we revealed that the yield of CsPbI₃ QDs is mainly dependent on Pb/Cs ratio. The Pb/I ratio can affect phase purity and dispersibility of QDs but shows a negligible effect on the reaction yield (Figure S6, Supporting Information).

The flexibility in precursors tuning enables the investigation of the effect of precursor ratios on the properties and photovoltaic performance of CsPbI₃ QDs. A Pb/Cs input ratio of 2 was chosen because under this condition we can obtain both decent synthetic yield and phase-pure CsPbI₃ QDs with Pb/I ratio ranging from 1:2 to 1:5. As shown in Figure 2a–d, the shape and size distribution of the CsPbI₃ QDs synthesized with different Pb/I input ratios are characterized by transmission electron microscopy (TEM). All the obtained CsPbI₃ QDs show the typical cubic shape with similar size of ≈15 nm. No significant differences in size distribution can be detected as revealed by the size histograms. The powder X-ray diffraction (XRD) patterns of the CsPbI₃ QDs can be well indexed to the orthorhombic γ phase without any additional phases (Figure 2e).^[44] As shown in Figure 2f, all the CsPbI₃ QDs exhibit the same absorption edge at 670 nm. The photoluminescence (PL) peak positions (688 nm) and the FWHM of all tested samples also display negligible differences with varied Pb/I ratios, consistent with their similar size and size distribution in Figure 2a–d. And, the obtained QDs show decent air stability (Figure S7, Supporting Information). The dynamic PL lifetime of these CsPbI₃ QDs in hexane was further measured using time-resolved photoluminescence (TRPL). As shown in Figure 2g and Table S5, Supporting Information, a monotonic increase in the average PL lifetime from 14.4 ns (Pb: I = 1:2) to 61.3 ns (Pb: I = 1:5) was observed with increasing iodide input. Since the measured CsPbI₃ QDs possess a very similar size. The PL lifetime can reflect the amount of nonradiative sites on the surface. The improved PL lifetime of the QDs synthesized with higher iodide implies the iodide-rich condition can suppress the formation of recombination pathways on the surface of the CsPbI₃ QDs.^[45] The absolute PLQY of these CsPbI₃ QDs was measured as well. We notice that higher iodide feeding results in improved PLQY (Figure 2h), which is in good agreement with the PL lifetime results. In short, the synthesis with higher iodide input can produce CsPbI₃ QDs with better surface passivation. It is worth mentioning that the PLQY values of our CsPbI₃ QDs are relatively lower than the reported ones^[45,46] in which the QDs were only purified by direct centrifugation without ligand removal by destructive antisolvents. In contrast, our QDs were purified rigorously to achieve high photovoltaic performance (Figure S4, Supporting Information), which requires significant removal of surface ligands, leading to reduced PLQY.

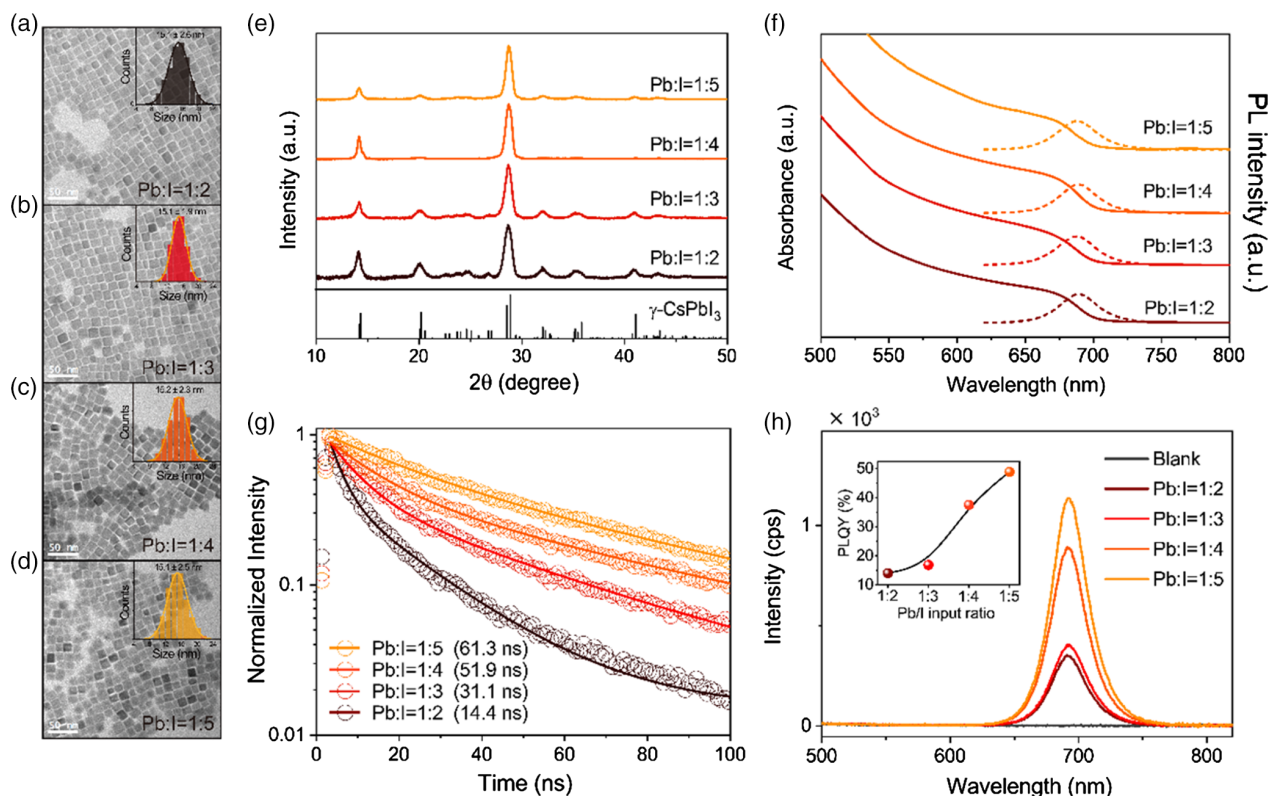


Figure 2. a–d) TEM images of the CsPbI₃ QDs synthesized with different Pb/I input ratios. The size distribution histogram is inserted in each graph. e) XRD, f) UV–visible and PL spectra, g) TRPL decay, and h) PLQY of CsPbI₃ QDs synthesized with different Pb/I input ratios. The Pb/Cs ratio is fixed at 2.

To uncover the reason for the improved passivation of CsPbI₃ QDs synthesized under iodide-rich conditions, Fourier-transform infrared spectroscopy (FTIR) and X-ray photoelectron spectroscopy (XPS) were performed to probe their surface chemistry. The FTIR samples were prepared by spin coating the purified CsPbI₃ QDs on calcium fluoride (CaF₂) substrate with the same concentration. The FTIR samples are shown in **Figure 3a**, the vibrational modes at $\nu(\text{C} - \text{H}_x) = 2768\text{--}2986\text{ cm}^{-1}$, $\nu(\text{C} = \text{C} - \text{H}) = 3005\text{ cm}^{-1}$ are attributed to oleyl group from both OA and OLA. The broad resonance centered at 3138 cm^{-1} ($\nu(\text{N} - \text{H}_3^+)$) is due to stretching vibrations of ammonium groups. A monotonic increase in the FTIR intensity at both the region of $\nu(\text{N} - \text{H}_3^+)$ and $\nu(\text{C} - \text{H}_x)$ is observed at increased Pb/I ratio, indicating more OLA bound on the QDs synthesized with higher iodide input. This result can be confirmed by the XPS results. As shown in **Figure 3b**, the intensities of C 1s and N 1s peaks increase for the CsPbI₃ QDs synthesized at higher iodide feeding. To investigate the correlation between the feeding precursor ratios and the actual elemental ratios in the obtained QDs, we performed XPS measurements on Cs, Pb, and I (**Figure S8**, Supporting Information), with the extracted results shown in **Figure 3c**. As the Pb:I ratio increases from 1:2 to 1:5, the atomic I/Pb ratio in the QDs increases from 3.99 to 4.24. Meanwhile, the atomic Cs/Pb ratio decreases from 1.60 to 1.32. Collectively, we speculate that the precursor input ratio can alter the surface bonding motifs of the synthesized CsPbI₃ QDs. As schematically shown in **Figure 3d**, with the increase in iodine

supply, the iodine vacancies on the QD surface can be filled. Meanwhile, the accompanying counterion, i.e., oleylammonium (OLA⁺), increases as well, which substitutes surface Cs⁺ ions to form a more stable surface configuration. The substitution of surface Cs⁺ with OLA⁺ has been demonstrated thermodynamically favorable due to the formation of three hydrogen bonds between the $-\text{NH}_3^+$ moiety and the surrounding I⁻ ions on the surface of the NCs, compared to the case that OLA⁺ absorbs on the surface as ligand with only one hydrogen bond.^[47] The fill of surface iodine vacancies and enhanced binding of OLA⁺ can result in improved optical properties.^[5,39,48]

Finally, the photovoltaic performances of CsPbI₃ QDs synthesized by the ternary-precursor strategy were investigated using the device structure of glass/fluorine-doped tin dioxide (FTO)/TiO₂ (40 nm)/CsPbI₃ QDs (450 nm)/poly(triarylamine) (PTAA) (80 nm)/MoO₃ (8 nm)/Ag (100 nm) (**Figure 4a**). Each constituent layer of the device can be identified in the cross-sectional scanning electron microscopy (SEM) image (**Figure 4b**). Since the photovoltaic application requires semiconductive QD film with high carrier mobility, we treated the QD layer with the standard MeOAc procedure to remove surface ligands.^[12] However, we found that the treated QD layer can be partly washed off during the deposition of the subsequent layer as the Pb:I precursor ratio approaches 1:3. The issue becomes more serious for the QDs with higher iodide input, indicating that the standard MeOAc treatment cannot effectively remove the surface ligands on the CsPbI₃ QDs synthesized by ternary-precursor strategy. As shown

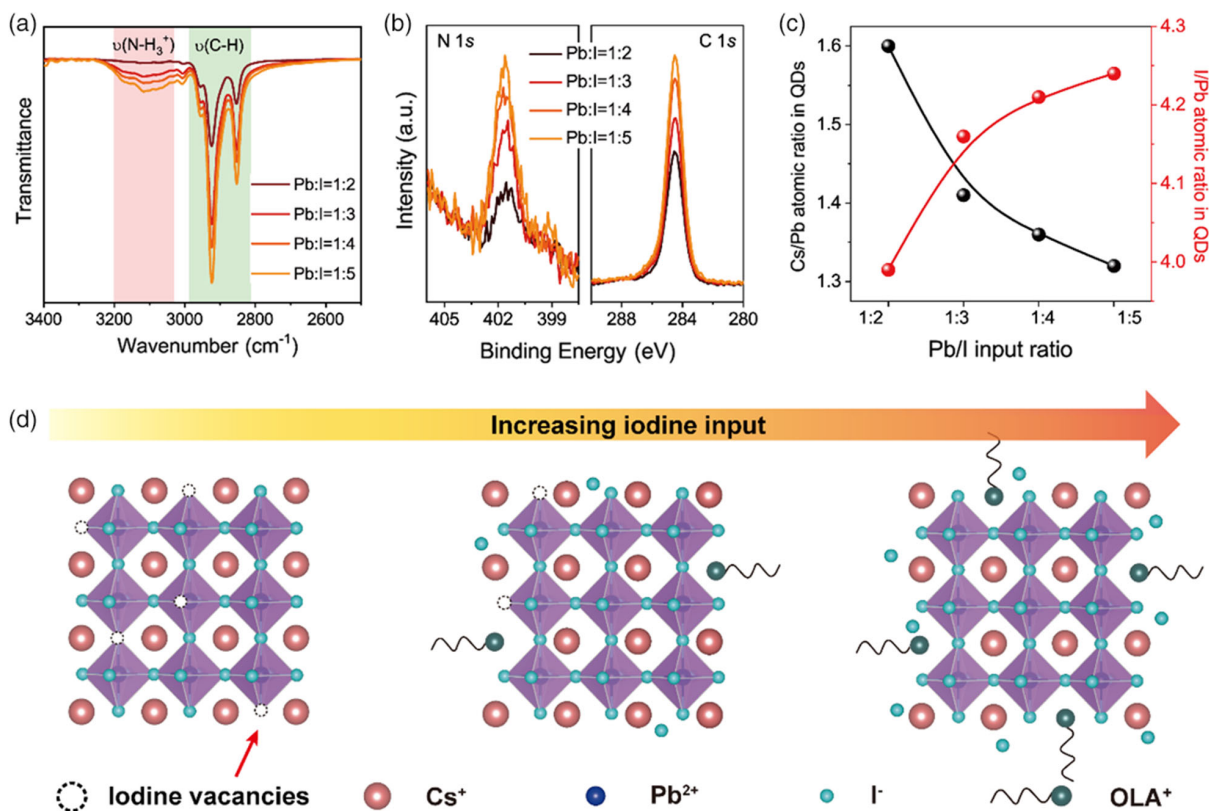


Figure 3. a) FTIR spectra, b) N 1s and C 1s XPS spectra, and c) atomic elemental ratio of CsPbI₃ QDs synthesized with different Pb/I input ratios. The Pb/Cs ratio is fixed at 2. d) Illustrations of the effect of the Pb/I input ratio on the surface termination of the CsPbI₃ QDs.

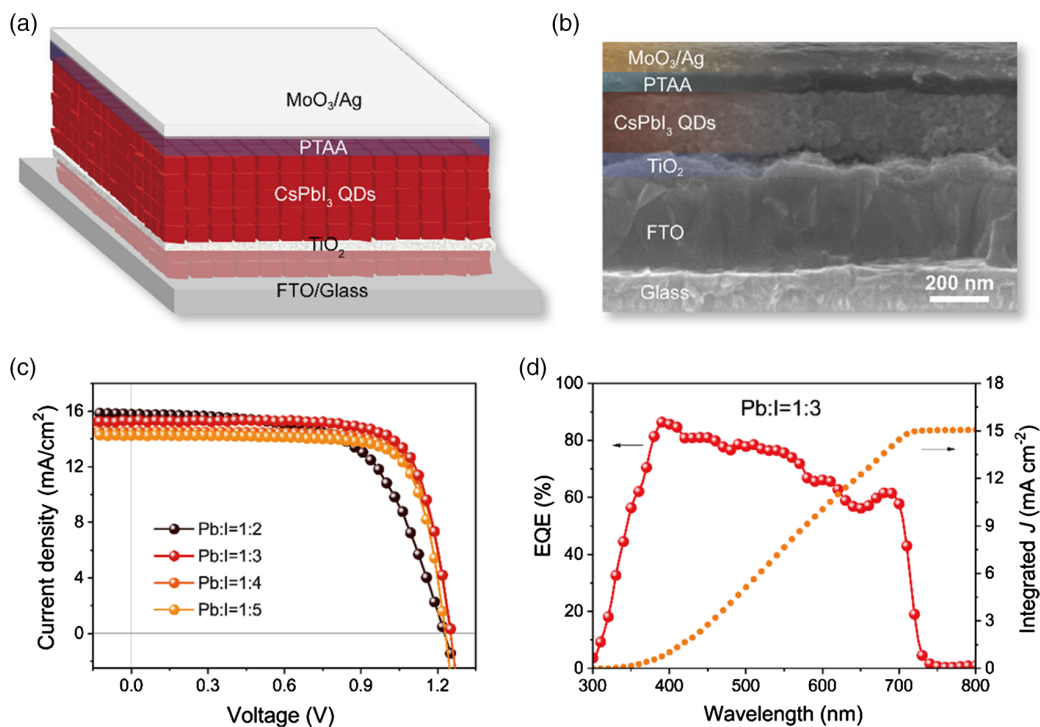


Figure 4. a) Schematic and b) cross-sectional SEM image of the CsPbI₃ QD solar cell. c) Current–voltage characteristics of the solar cells based on the CsPbI₃ QD synthesized with different Pb/I input ratios. The Pb/Cs ratio is fixed at 2. d) EQE spectra of the champion device.

Table 1. Device parameters of solar cells based on CsPbI₃ QDs synthesized with different Pb/I input ratios, measured under the reverse scan.

| Pb: I | | V _{oc} [V] | J _{sc} [mA cm ⁻²] | FF | PCE [%] |
|-------|-----------------------|---------------------|--|----------------|---------------|
| 1:2 | Average ^{a)} | 1.208 (±0.009) | 15.19 (±0.05) | 0.603 (±0.021) | 11.07 (±0.43) |
| | Champion | 1.218 | 15.78 | 0.615 | 11.82 |
| 1:3 | Average ^{a)} | 1.231 (±0.005) | 14.52 (±0.45) | 0.733 (±0.012) | 13.10 (±0.50) |
| | Champion | 1.238 | 15.22 | 0.756 | 14.24 |
| 1:4 | Average ^{a)} | 1.230 (±0.012) | 14.11 (±0.30) | 0.756 (±0.005) | 13.12 (±0.40) |
| | Champion | 1.248 | 14.53 | 0.755 | 13.69 |
| 1:5 | Average ^{a)} | 1.220 (±0.009) | 14.15 (±0.29) | 0.745 (±0.010) | 12.86 (±0.31) |
| | Champion | 1.218 | 14.27 | 0.767 | 13.33 |

^{a)}The average values were summarized from 20 parallel devices for each condition.

in Figure S9, Supporting Information, QDs with more iodide feeding exhibit higher residual of alkyl-chain ligands after being treated by MeOAc, which can hinder charge transport and result in unsatisfactory device performance. We attribute it to the enhanced hydrogen bonding between OLA⁺ and the surface of QDs synthesized by the ternary-precursor strategy.^[47] To efficiently remove the insulating ligands, di-n-propylamine (DPA) and guanidinium (GA⁺) treatment were used, which can realize surface ligand removal and passivation simultaneously, demonstrated by our previous works.^[25,42] As shown in Figure S10, Supporting Information, the surface ligands can be substantially removed after using the DPA and GA⁺ treatment. The current density–voltage (*J*–*V*) characteristics of the optimized solar cells based on CsPbI₃ QDs synthesized with different Pb/I input ratios are shown in Figure 4c and Table 1. After finely optimizing the concentration of DPA and GA⁺ (Table S6, Supporting Information), a champion PCE up to 14.24% can be achieved under an optimal Pb:I ratio of 1:3, with a V_{oc} of 1.238 V, a J_{sc} of 15.22 mA cm⁻², and a fill factor (FF) of 0.756. As shown in Figure 4d, the integrated J_{sc} value from the external quantum efficiencies (EQE) curve under the AM 1.5G solar spectrum for the champion device is 15.09 mA cm⁻², which is consistent with the measured J_{sc} value. To verify the reliability of the results, we fabricated several individual devices for each condition and the PCE distribution is shown in Figure S11, Supporting Information, which shows good repeatability. Our results not only demonstrate a controllable strategy to expand the yields of CsPbI₃ QDs but also show potential photovoltaic applications with decent PCEs that is comparable with the ones based on traditional binary-precursor method (≈15%).^[25,42] Future improvement in solar cell performance should focus on the surface ligand management to fully remove the insulating ligands and simultaneously improve surface passivation.

3. Conclusion

In conclusion, we systematically investigated the effect of precursor ratios on the reaction yield of CsPbI₃ QDs and their optoelectronic properties using the ternary-precursor synthesis. We reveal that under I-rich conditions, pure-phase CsPbI₃ QDs can be obtained for different Pb/Cs input ratios. In addition,

the ternary-precursor method can maximize the conversion (Pb/Cs = 1) of the cation precursor. Resultantly, the reaction yield is more than 7.5 times higher than the conventional binary-precursor method under the same Pb input. Accordingly, the cost for the preparation of CsPbI₃ QDs can be reduced from ≈303 \$ g⁻¹ to as low as 42 \$ g⁻¹. Under the same Pb/Cs ratio, the optical properties of the QDs can be improved by increasing the iodide feeding. Furthermore, the obtained CsPbI₃ QDs were applied to fabricate QD solar cells, showing a PCE of 14.24%, which is close to the reported state-of-the-art CsPbI₃ QDs photovoltaic devices. Our results indicate that the design of synthetic protocol can improve reaction yield, reduce material cost, and enhance optoelectronic properties of CsPbI₃ QDs, which can shed light on the future large-scale manufacturing of perovskite QD-based applications.

4. Experimental Section

Chemicals: Cs₂CO₃ (99.9%, J&K), NH₄I (99%, J&K), PbAc₂·3H₂O (99%, Alfa), OA (90%, Aldrich), OLA (70%, Aldrich), ODE (90%, J&K), *n*-hexane (97.5%, J&K), methyl acetate (MeOAc, anhydrous 99.5%, J&K), *n*-octane (anhydrous, ≥98%, Alfa), ethyl acetate (EtOAc, anhydrous, 99.8%, Sigma), toluene (analytical reagent, 98%, Chinasun Specialty Products Co.,Ltd.), PTAA (Xi'an Polymer Light Technology Corp.), and guanidinium thiocyanate (GASCN, Xi'an Polymer Light Technology Corp.) were used. All the chemicals were used as received without further purification.

Preparation of Iodide Precursor: A mixture of NH₄I (3.48 g, 24 mmol) and OLA (10 mL) was loaded into a 25 ml three-neck flask. The solution was heated and stirred at 90 °C under N₂ until NH₄I is fully dissolved. Then, the solution was vacuumed for 30 min at 90 °C. The obtained solution was stored in an N₂ filled glove box, and heated to 100 °C before use.

Synthesis of CsPbI₃ QDs: A mixture of PbAc₂·3H₂O (0.82 g, 2.16 mmol), Cs₂CO₃ (0.18 g, 0.54 mmol), OA (5 mL), OLA (3.2 ml, 2.3 ml, 1.4 ml, and 0.5 ml for Pb:I ratio of 1:2, 1:3, 1:4, and 1:5, respectively), and ODE (50 mL) was loaded into a 250 mL three-neck flask. The solution was heated and stirred at 90 °C and degassed until PbAc₂·3H₂O and Cs₂CO₃ had been completely solubilized. Then, the temperature was raised to 180 °C under N₂, and iodide precursor solution (1.8, 2.7, 3.6, and 4.5 ml for Pb:I ratio of 1:2, 1:3, 1:4, and, 1:5, respectively) was quickly injected and the reaction mixture was cooled by the ice-water bath after 5 s.

Isolation and Purification of CsPbI₃ QDs: The crude solution of QDs was precipitated by adding MeOAc (MeOAc: ODE = 3:1 by volume), and the mixture was centrifuged at 8000 rpm for 5 min. The supernatant was discarded, and the precipitate was redispersed in 18 mL hexane. Then, the solution was mixed with 18 mL MeOAc and centrifuged for 3 min at

8000 rpm. The supernatant was discarded, and the precipitate was redispersed in 20 mL hexane. Finally, the solution was centrifuged at 4000 rpm for 5 min to remove large aggregates, and the supernatant was collected. After being dried through a rotary evaporator, the QD solids were weighed to obtain the synthetic production.

Characterization of Materials: The UV–vis absorption spectra, PL spectra, Fourier transform infrared spectrum, and time-resolved decay PL spectra of purified CsPbI₃ QDs solution were measured by Perkin Elmer model Lambda 750 spectrophotometer, FluoroMax-4 spectrofluorometer (HORIBA Scientific), Bruker HYPERION FTIR spectrometer, and Hamamatsu streak camera, respectively. All the PLQY values were absolute quantum yields that were obtained by ultraviolet–near infrared (UV–NIR) absolute PL quantum yield spectrometer C13534 (HAMAMATSU). TEM images were taken by Tecnai G2 F20 S-Twin transmission electron microscope operated at 200 kV. XRD patterns were determined by Rigaku D/Max-Ra X-ray diffractometer with monochrome at Cu K α radiation ($\lambda \approx 1.54 \text{ \AA}$). The XPS was measured by a Kratos AXIS Ultra DLD ultrahigh vacuum photoemission spectroscopy system, with an Al K α radiation source.

CsPbI₃ QDs Solar Cells Fabrication and Characterization: CsPbI₃ QDs solar cells were fabricated based on the device structure of FTO/TiO₂ (40 nm)/CsPbI₃ QDs (450 nm)/PTAA (80 nm)/MoO₃ (8 nm)/Ag (100 nm). Compact TiO₂ films ($\approx 40 \text{ nm}$) were deposited onto the cleaned FTO substrates using chemical bath deposition at 70 °C. The films were dried at 200 °C for 30 min and then exposed to UV–ozone for 10 min.^[49] The CsPbI₃ QDs solution (70 mg mL⁻¹ in octane) was spin cast on the substrate at 1000 rpm for 20 s and 2000 rpm for 15 s. Then, 120 μ L of neat MeOAc or the solution of DPA in MeOAc was dropped on the as-cast CsPbI₃ QDs layer for 5 s to remove long chain ligands and then spun at 2000 rpm for 20 s. This process was repeated five times to build up a QD film with the desired thickness ($\approx 450 \text{ nm}$). Then, the film was immersed into the solution of GASCN in EtOAc and rinsed with neat MeOAc, and dried by N₂. The detailed concentrations of DPA and GASCN were summarized in Table S5, Supporting Information. This QDs film fabrication process was conducted in a dry air-filled glove box at room temperature with relative humidity below 10%. PTAA solution (15 mg mL⁻¹ in toluene) doped with tris(pentafluorophenyl)borane (dopant/PTAA = 5% in weight) was spin coated on top of the QD films at 3000 rpm for 40 s.^[50] No extra oxidation or heating process was conducted for the PTAA layer ($\approx 80 \text{ nm}$). The QD solar cells were completed after subsequent thermal evaporation of 8 nm of MoO₃ and 100 nm of Ag under a vacuum of $< 1 \times 10^{-6}$ mbar. The active area of the devices was 7.25 mm² determined by a shadow metal mask. The J–V characteristics of the devices were acquired using a Keithley 2400 digital source meter under simulated AM 1.5 G spectrum at 100 mW cm⁻² with a solar simulator (Class AAA, 94023 A-U, Newport). The light intensity had been calibrated to 100 mW cm⁻² by a monocrystalline silicon reference cell (91 150 V, Newport Oriel).

Supporting Information

Supporting Information is available from the Wiley Online Library or from the author.

Acknowledgements

Y.Q. and Y.S. contributed equally to this work, conceived the idea, and contributed to most experimental work. This work was supported by the National Key Research Projects (Grant No. 2016YFA0202402), the National Natural Science Foundation of China (Grant Nos. 52002260, 51803144, and 61674111), the Natural Science Foundation of Jiangsu Province of China (BK20200872), and “111” projects. The authors thank the Collaborative Innovation Center of Suzhou Nano Science and Technology, Soochow University, the Priority Academic Program Development of Jiangsu Higher Education Institutions (PAPD). The Project was also supported by the State Key Laboratory of applied optics (Grant No. SKLAO2020001A03).

Conflict of Interest

The authors declare no conflict of interest.

Data Availability Statement

The data that support the findings of this study are available from the corresponding authors upon reasonable request.

Keywords

CsPbI₃ quantum dots, material cost, surface chemistry, synthetic production, yields

Received: February 3, 2021

Revised: March 17, 2021

Published online: April 9, 2021

- [1] M. V. Kovalenko, L. Protesescu, M. I. Bodnarchuk, *Science* **2017**, *358*, 745.
- [2] Q. A. Akkerman, G. Raino, M. V. Kovalenko, L. Manna, *Nat. Mater.* **2018**, *17*, 394.
- [3] Q. Zhang, Y. Yin, *ACS Cent. Sci.* **2018**, *4*, 668.
- [4] D. Yang, M. Cao, Q. Zhong, P. Li, X. Zhang, Q. Zhang, *J. Mater. Chem. C* **2019**, *7*, 757.
- [5] J. Shamsi, A. S. Urban, M. Imran, L. De Trizio, L. Manna, *Chem. Rev.* **2019**, *119*, 3296.
- [6] A. Swarnkar, R. Chulliyil, V. K. Ravi, M. Irfanullah, A. Chowdhury, A. Nag, *Angew. Chem., Int. Ed.* **2015**, *54*, 15424.
- [7] K. Chen, Q. Zhong, W. Chen, B. Sang, Y. Wang, T. Yang, Y. Liu, Y. Zhang, H. Zhang, *Adv. Funct. Mater.* **2019**, *29*, 1900991.
- [8] H. Wang, X. Gong, D. Zhao, Y.-B. Zhao, S. Wang, J. Zhang, L. Kong, B. Wei, R. Quintero-Bermudez, O. Voznyy, Y. Shang, Z. Ning, Y. Yan, E. H. Sargent, X. Yang, *Joule* **2020**, *4*, 1977.
- [9] H. Wang, Y. Dou, P. Shen, L. Kong, H. Yuan, Y. Luo, X. Zhang, X. Yang, *Small* **2020**, *16*, 2001062.
- [10] C. Zhang, S. Wang, X. Li, M. Yuan, L. Turyanska, X. Yang, *Adv. Funct. Mater.* **2020**, *30*, 1910582.
- [11] C. Zhang, J. Chen, S. Wang, L. Kong, S. W. Lewis, X. Yang, A. L. Rogach, G. Jia, *Adv. Mater.* **2020**, *32*, 2002736.
- [12] A. Swarnkar, A. R. Marshall, E. M. Sanehira, B. D. Chernomordik, D. T. Moore, J. A. Christians, T. Chakrabarti, J. M. Luther, *Science* **2016**, *354*, 92.
- [13] Y. Wang, M. I. Dar, L. K. Ono, T. Zhang, M. Kan, Y. Li, L. Zhang, X. Wang, Y. Yang, X. Gao, Y. Qi, M. Gratzel, Y. Zhao, *Science* **2019**, *365*, 591.
- [14] Q. Tai, K.-C. Tang, F. Yan, *Energy Environ. Sci.* **2019**, *12*, 2375.
- [15] L. N. Zhang, C. T. Kang, G. Z. Zhang, Z. X. Pan, Z. S. Huang, S. H. Xu, H. S. Rao, H. B. Liu, S. F. Wu, X. Wu, X. S. Li, Z. L. Zhu, X. H. Zhong, A. K. Y. Jen, *Adv. Funct. Mater.* **2021**, *31*, 2005930.
- [16] M. Hao, Y. Bai, S. Zeiske, L. Ren, J. Liu, Y. Yuan, N. Zarrabi, N. Cheng, M. Ghasemi, P. Chen, M. Lyu, D. He, J.-H. Yun, Y. Du, Y. Wang, S. Ding, A. Armin, P. Meredith, G. Liu, H.-M. Cheng, L. Wang, *Nat. Energy* **2020**, *5*, 79.
- [17] Q. Zhao, A. Hazarika, X. Chen, S. P. Harvey, B. W. Larson, G. R. Teeter, J. Liu, T. Song, C. Xiao, L. Shaw, M. Zhang, G. Li, M. C. Beard, J. M. Luther, *Nat. Commun.* **2019**, *10*, 2842.
- [18] F. Li, S. Zhou, J. Yuan, C. Qin, Y. Yang, J. Shi, X. Ling, Y. Li, W. Ma, *ACS Energy Lett.* **2019**, *4*, 2571.

- [19] E. M. Sanehira, A. R. Marshall, J. A. Christians, S. P. Harvey, P. N. Ciesielski, L. M. Wheeler, P. Schulz, L. Y. Lin, M. C. Beard, J. M. Luther, *Sci. Adv.* **2017**, *3*, eaao4204.
- [20] J. Yuan, X. Ling, D. Yang, F. Li, S. Zhou, J. Shi, Y. Qian, J. Hu, Y. Sun, Y. Yang, X. Gao, S. Duhm, Q. Zhang, W. Ma, *Joule* **2018**, *2*, 2450.
- [21] Q. Wang, Z. Jin, D. Chen, D. Bai, H. Bian, J. Sun, G. Zhu, G. Wang, S. Liu, *Adv. Energy Mater.* **2018**, *8*, 1800007.
- [22] F. Liu, C. Ding, Y. Zhang, T. Kamisaka, Q. Zhao, J. M. Luther, T. Toyoda, S. Hayase, T. Minemoto, K. Yoshino, B. Zhang, S. Dai, J. Jiang, S. Tao, Q. Shen, *Chem. Mater.* **2019**, *31*, 798.
- [23] X. F. Ling, S. J. Zhou, J. Y. Yuan, J. W. Shi, Y. L. Qian, B. W. Larson, Q. Zhao, C. C. Qin, F. C. Li, G. Z. Shi, C. Stewart, J. X. Hu, X. L. Zhang, J. M. Luther, S. Duhm, W. L. Ma, *Adv. Energy Mater.* **2019**, *9*, 1900721.
- [24] J. Kim, B. Koo, W. H. Kim, J. Choi, C. Choi, S. J. Lim, J. S. Lee, D. H. Kim, M. J. Ko, Y. Kim, *Nano Energy* **2019**, *66*, 104130.
- [25] X. Ling, J. Yuan, X. Zhang, Y. Qian, S. M. Zakeeruddin, B. W. Larson, Q. Zhao, J. Shi, J. Yang, K. Ji, Y. Zhang, Y. Wang, C. Zhang, S. Duhm, J. M. Luther, M. Gratzel, W. Ma, *Adv. Mater.* **2020**, *32*, e2001906.
- [26] J. Shi, F. Li, Y. Jin, C. Liu, B. Cohen-Kleinstejn, S. Yuan, Y. Li, Z. K. Wang, J. Yuan, W. Ma, *Angew. Chem., Int. Ed.* **2020**, *59*, 22230.
- [27] Y. F. Wang, B. Y. Jia, J. Wang, P. Y. Xue, Y. Q. Xiao, T. F. Li, J. Y. Wang, H. Lu, Z. Tang, X. H. Lu, F. Huang, X. W. Zhan, *Adv. Mater.* **2020**, *32*, 2002066.
- [28] K. Chen, W. Jin, Y. Zhang, T. Yang, P. Reiss, Q. Zhong, U. Bach, Q. Li, Y. Wang, H. Zhang, *J. Am. Chem. Soc.* **2020**, *142*, 3775.
- [29] D. Jia, J. Chen, M. Yu, J. Liu, E. M. J. Johansson, A. Hagfeldt, X. Zhang, *Small* **2020**, *16*, e2001772.
- [30] C. H. Bi, X. J. Sun, X. Huang, S. X. Wang, J. F. Yuan, J. X. Wang, T. Pullerits, J. J. Tian, *Chem. Mater.* **2020**, *32*, 6105.
- [31] L. Protesescu, S. Yakunin, M. I. Bodnarchuk, F. Krieg, R. Caputo, C. H. Hendon, R. X. Yang, A. Walsh, M. V. Kovalenko, *Nano Lett.* **2015**, *15*, 3692.
- [32] I. Lignos, S. Stavrakis, G. Nedelcu, L. Protesescu, A. J. deMello, M. V. Kovalenko, *Nano Lett.* **2016**, *16*, 1869.
- [33] F. Li, Y. Liu, H. Wang, Q. Zhan, Q. Liu, Z. Xia, *Chem. Mater.* **2018**, *30*, 8546.
- [34] P. Liu, W. Chen, W. Wang, B. Xu, D. Wu, J. Hao, W. Cao, F. Fang, Y. Li, Y. Zeng, R. Pan, S. Chen, W. Cao, X. W. Sun, K. Wang, *Chem. Mater.* **2017**, *29*, 5168.
- [35] Q. Wang, Y. C. Shao, H. P. Xie, L. Lyu, X. L. Liu, Y. L. Gao, J. S. Huang, *Appl. Phys. Lett.* **2014**, *105*, 163508.
- [36] B. Danekamp, C. Muller, M. Sendner, P. P. Boix, M. Sessolo, R. Lovrincic, H. J. Bolink, *J. Phys. Chem. Lett.* **2018**, *9*, 2770.
- [37] P. Cui, D. Wei, J. Ji, H. Huang, E. Jia, S. Dou, T. Wang, W. Wang, M. Li, *Nat. Energy* **2019**, *4*, 150.
- [38] M. Imran, V. Caligiuri, M. Wang, L. Goldoni, M. Prato, R. Krahn, L. De Trizio, L. Manna, *J. Am. Chem. Soc.* **2018**, *140*, 2656.
- [39] A. Dutta, R. K. Behera, P. Pal, S. Baitalik, N. Pradhan, *Angew. Chem., Int. Ed.* **2019**, *58*, 5552.
- [40] Y. T. Cai, H. R. Wang, Y. Li, L. Wang, Y. Lv, X. Y. Yang, R. J. Xie, *Chem. Mater.* **2019**, *31*, 881.
- [41] E. Yassitepe, Z. Yang, O. Voznyy, Y. Kim, G. Walters, J. A. Castañeda, P. Kanjanaboos, M. Yuan, X. Gong, F. Fan, J. Pan, S. Hoogland, R. Comin, O. M. Bakr, L. A. Padilha, A. F. Nogueira, E. H. Sargent, *Adv. Funct. Mater.* **2016**, *26*, 8757.
- [42] Y. Wang, J. Yuan, X. Zhang, X. Ling, B. W. Larson, Q. Zhao, Y. Yang, Y. Shi, J. M. Luther, W. Ma, *Adv. Mater.* **2020**, *32*, e2000449.
- [43] Y. Zhang, T. D. Siegler, C. J. Thomas, M. K. Abney, T. Shah, A. De Gorostiza, R. M. Greene, B. A. Korgel, *Chem. Mater.* **2020**, *32*, 5410.
- [44] Q. Zhao, A. Hazarika, L. T. Schelhas, J. Liu, E. A. Gaulding, G. Li, M. Zhang, M. F. Toney, P. C. Sercel, J. M. Luther, *ACS Energy Lett.* **2019**, *5*, 238.
- [45] F. Liu, Y. Zhang, C. Ding, S. Kobayashi, T. Izuishi, N. Nakazawa, T. Toyoda, T. Ohta, S. Hayase, T. Minemoto, K. Yoshino, S. Dai, Q. Shen, *ACS Nano* **2017**, *11*, 10373.
- [46] X. Shen, Y. Zhang, S. V. Kershaw, T. Li, C. Wang, X. Zhang, W. Wang, D. Li, Y. Wang, M. Lu, L. Zhang, C. Sun, D. Zhao, G. Qin, X. Bai, W. W. Yu, A. L. Rogach, *Nano Lett.* **2019**, *19*, 1552.
- [47] V. K. Ravi, P. K. Santra, N. Joshi, J. Chugh, S. K. Singh, H. Rensmo, P. Ghosh, A. Nag, *J. Phys. Chem. Lett.* **2017**, *8*, 4988.
- [48] N. Pradhan, A. Dutta, S. K. Dutta, S. Das Adhikari, *Angew. Chem., Int. Ed.* **2018**, *57*, 9083-9087.
- [49] A. Yella, L. P. Heiniger, P. Gao, M. K. Nazeeruddin, M. Gratzel, *Nano Lett.* **2014**, *14*, 2591.
- [50] J. Luo, J. Xia, H. Yang, L. Chen, Z. Wan, F. Han, H. A. Malik, X. Zhu, C. Jia, *Energy Environ. Sci.* **2018**, *11*, 2035.